Special Issue: DTD 2006 in JAPAN
Original Article
J. Jpn. Soc. Microgravity Appl. Vol. 24 No. 3 2007 (241-245)

Flame Spread of N-Decane Droplet Array with Pre-Evaporation in Microgravity

Masao KIKUCHI[1], Shin YAMAMOTO[1], Shinichi YODA[1] and Masato MIKAMI[2]

[1] Japan Aerospace Exploration Agency, Tsukuba, Japan, kikuchi.masao@jaxa.jp
[2] Yamaguchi University, Ube, Japan, mmikami@yamaguchi-u.ac.jp

Abstract

Flame spread phenomena of linear n-decane droplet array are investigated by microgravity experiments and numerical analysis. Especially, pre-evaporation effects of droplets on flame spread process are examined in this study. In microgravity experiments, each droplet which consists of the array is formed and sustained at intersections of fine, X-shaped SiC fibers of 14 micrometer diameter. Activation delay time of the igniter wire after insert of the array into the combustion chamber, t_w, is employed as primary experimental parameter to control the degree of pre-evaporation of the array. Experiments are performed with some different droplet diameter (d_0) and droplet interval (S) at ambient air with T = 600 K. Experimental results showed development of blue flame at spreading flame front with enhancement of pre-evaporation. Also, OH radical emission showed characteristic shape at flame front region when pre-evaporation of droplets are developed. Flame spread rate V_f increased with increase in the degree of pre-evaporation. However, V_f appears to approach some value with further pre-evaporation. In addition, numerical results showed similar characteristic flame structure at flame front as experimental results. It was suggested the flame front has a structure like a triple flame.

1. Introduction

Flame spread phenomena of a fuel droplet array have been investigated by researchers [1-8]. Flame spread of linear droplet array is the simplest configuration to study flame spread mechanism among droplets of fuel spray. Therefore, fundamental research on flame spread of fuel droplet array is expected to provide basic but essential knowledge on flame propagation mechanism of fuel spray. Also, flame spread among fuel droplets would occur in formation process of group flame which surrounds multiple droplets.

In addition, microgravity environment enables us to observe the phenomena without the effect of natural convection which causes difficulties apart from inherent complexity of combustion phenomena.

The authors have studied flame spread of a n-decane droplet array by microgravity experiments [4,5] as well as numerical simulation [6,7], in accordance with theoretical consideration by Umemura [8]. In past research, we mainly investigated fundamental flame spread mechanism including the effect of droplet interval and ambient temperature. In these studies, pre-evaporation of droplets prior to flame spread was little. In real spray combustion, however, droplets among the gas mixture of air and fuel vapor which is generated by pre-evaporation of droplets will burn. Therefore, flame spread characteristics of fuel droplet array with pre-evaporation would show more useful insight into real spray combustion.

Here, we report the results of microgravity experiments on flame spread of n-decane droplet array with pre-evaporation. In addition, numerical simulation was conducted for comparison with experimental results and detail examination of flame spread mechanism.

2. Experimental Method

A 4.5s drop shaft of the Microgravity Laboratory of Japan (MGLAB) was employed for microgravity experiments in this study. Microgravity level provided by the drop shaft is approximately 10^{-5} G. A picture of the experimental apparatus and schematic of experimental method are shown in **Fig.1** and **2**, respectively. Fundamental method of the experiments is similar with our past experiments [4,5].

Each droplet which consists of a droplet array is formed and sustained at intersections of fine, X-shaped SiC fibers of 14 micrometer diameter. After generation of the drolet array at room temperature environment of 1G, the experimental apparatus on board a drop capsule will enter into microgravity environment. In microgravity, the array is inserted into the combustion chamber which was preheated and sustained at a desired high temperature (T). A K-type thermocouple, which measures gas temperature near the edge droplet, was employed for definition of T as well as feedback control of electric heaters inside the combustion chamber. An edge droplet of the array is ignited by igniter wire and subsequent flame spread process is observed.

In this study, activation delay time of the igniter wire after insert of the array into the combustion chamber, t_w, is employed as primary experimental parameter to control the degree of pre-evaporation of the array. It would be reasonable assumption that the degree of pre-evaporation of droplets can be controlled by t_w, since evaporation rate of n-decane droplet at room temperature is small. Also, experiments are performed with some different

droplet diameter (d_0) and droplet interval (S) at ambient air with T = 600 K.

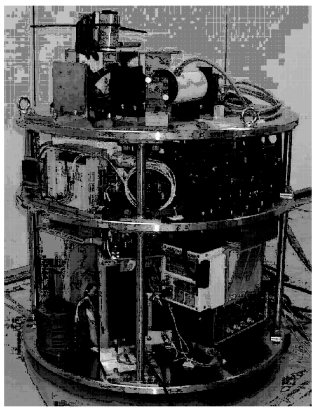

Fig.1 Experimental apparatus.

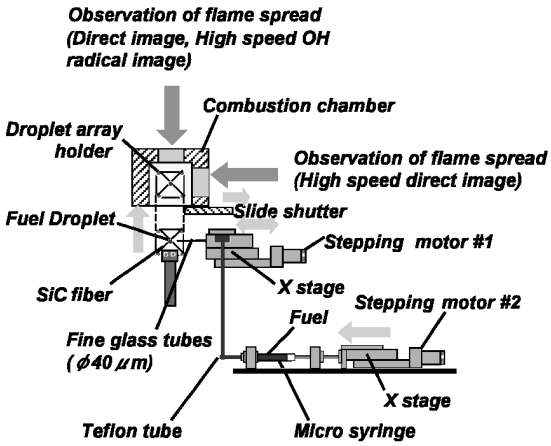

Fig.2 Schematic of experimental method.

Flame spread phenomena of the droplet array were observed by a high-speed video camera (500 fps) as well as a normal camcorder. In addition, OH radical emission was observed by using an optical system including an image intensifier, an interference filter (310 nm as the center wavelength, 10 nm as the half width) and another high-speed video camera (500 fps).

3. Experimental Results

Flame spread images obtained by normal camcorder are shown in **Fig.3, 4** and **5** for t_w = 0.1 s, 1.0 s and 1.7 s, respectively, with d_0 = 1.0 mm, S = 6 mm and T = 600 K. Here, t indicates the elapsed time after ignition of an edge droplet of the array.

In Fig.3 (a) and (b), spherical blue flame surrounding the 3rd and 4th droplet, followed by luminous flame which surrounds multiple droplets, are distinguishable. This type of flame spread is classified as "Mode III" in the classification by Umemura [8], since spherical blue flame at spreading flame front seems to be separated from burning flame behind the spherical flame in a moment of droplet ignition at flame front. In this case, spherical blue flame at spreading flame front increases its diameter with time and finally forms one luminous flame which surrounds multiple droplets [4,5].

In Fig.4 (b), on the other hand, spherical blue flame is not distinguishable. Instead, blue flame in a line state is clearly distinguishable at spreading flame front. The line state blue flame seems to cover almost 2 droplet intervals (S) in front of the luminous flame. Also, it is understood that flame spread rate would be larger than that of Fig.3, since blue flame at spreading flame front almost reaches the end of the array in just one frame (1/30 s) of camcorder images. Development of the blue flame at spreading flame front would be attributed to development of the flammable gas layer prior to flame spread by enhanced pre-evaporation of the droplets.

In Fig. 5 (b), blue flame in a line state reaches the end of the array in one frame of camcorder images. Therefore, it is suggested that flame spread rate would be large same as Fig.4.

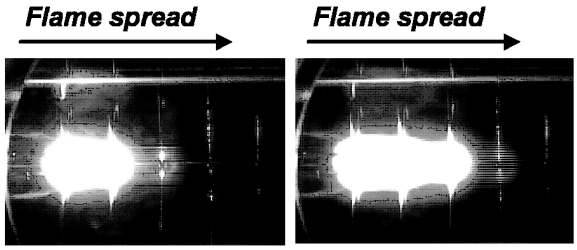

(a) t = 0.17 s (b) t = 0.23 s

Fig.3 Flame spread images obtained by a camcorder in microgravity.
(d_0 =1 mm, S = 6 mm, T = 600 K, t_w = 0.1 s)

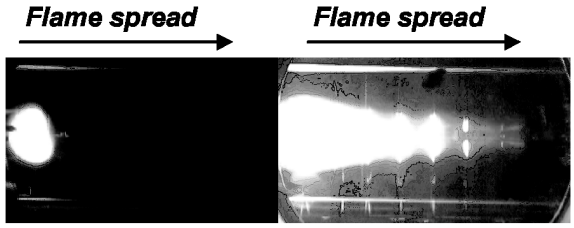

(a) t = 0 s (b) t = 0.03 s

Fig.4 Flame spread images obtained by a camcorder in microgravity.
(d_0 =1 mm, S = 6 mm, T = 600 K, t_w = 1.0 s)

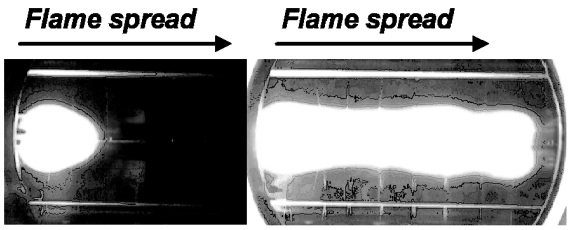

(a) t = 0 s (b) t = 0.03 s

Fig.5 Flame spread images obtained by a camcorder in microgravity.
(d_0 =1 mm, S = 6 mm, T = 600 K, t_w = 1.7 s)

Next, similar images obtained by normal camcorder are shown in **Fig.6 (a) ~ (c)** for t_w = 0.1 s, 1.0 s and 1.5 s, respectively, with d_0 = 0.5 mm, S = 3 mm and T = 600 K. Even at same t_w, in these cases, pre-evaporation of the droplet array would be more promoted than previous cases shown in Fig.3, 4 and 5, since heat capacity of each droplet is smaller and droplets vaporize faster. In addition, flammable gas layer formed around each droplet would connect more easily, since S is smaller than previous cases in S = 6 mm.

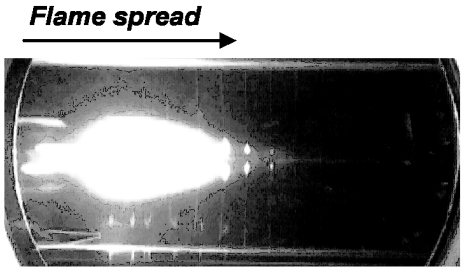

(a) t_w = 0.1 s (t = 0.03 s)

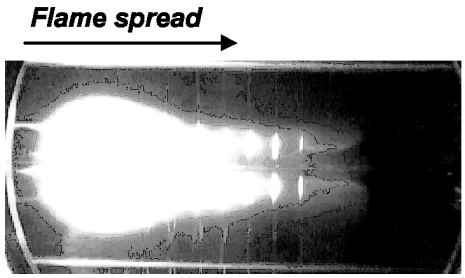

(b) t_w = 1.0 s (t = 0 s)

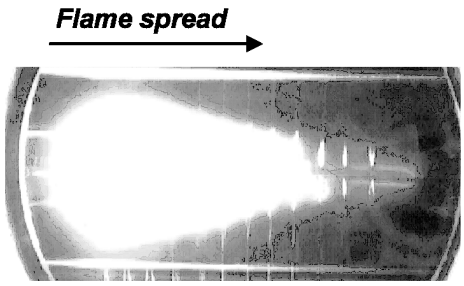

(c) t_w = 1.5 s (t = 0 s)

Fig.6 Flame spread images obtained by a camcorder in microgravity. (d_0 =0.5 mm, S = 3 mm, T = 600 K)

In Fig.6 (a), small spherical blue flame appears to exist at spreading flame front same as Fig.3, although it is not clear due to low magnification of the image. On the other hand, blue flame in a line state is clearly distinguishable at spreading flame front in Fig.6 (b) and (c). This would be due to development of premixed flame as a result of enhancement of pre-evaporation of the array. Also, increase of flame spread rate is suggested from Fig.6. Especially, flame spread rate seems to be very large in Fig.6 (b) and (c), since flame front immediately reaches far away from ignition point (left edge of the array in the images) after ignition of the edge droplet (t = 0 s).

Images of OH radical emission, correspond to the experimental conditions shown in Fig.3, 5 and 6, are shown in **Fig.7** and **8**. Approximate position of the center axis of the array is indicated in these figures for reference although it is difficult to indicate the position of each droplet. In Fig.7 (a), OH radical emission, corresponds to spherical droplet flame at the flame front as well as a group flame surrounding multiple droplets behind the spherical flame, can be seen. In Fig.7 (b), on the other hand, bow-shaped emission symmetrical with regard to the center axis of the array can be seen. The bow-shaped region roughly corresponds to premixed blue flame front.

In Fig.8 (a) ~ (c), characteristic bow-shaped emission is more clearly distinguishable than Fig. 7(b). In Fig.8 (b), especially, the bow-shaped emission of flame front as well as the emission corresponds to diffusion flame surrounding multiple droplets are both distinguishable. The bow-shaped emission becomes more distinguishable with development of flammable gas layer for larger t_w.

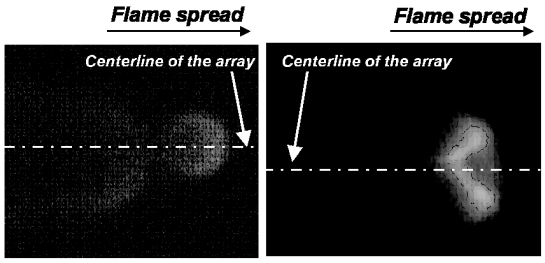

(a) t_w = 0.1 s (b) t_w = 1.7 s

Fig.7 Images of OH radical emission. (d_0 =1 mm, S = 6 mm, T = 600 K)

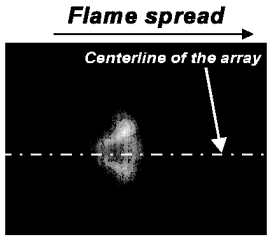

(a) t_w =0.1s

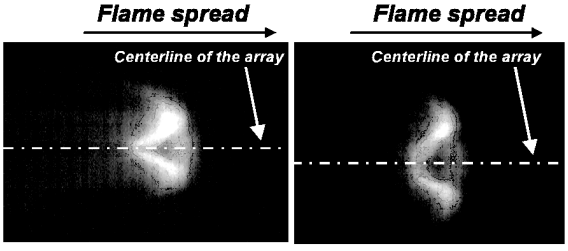

(b) t_w = 1.0 s (c) t_w = 1.5 s

Fig.8 Images of OH radical emission. (d_0 =0.5 mm, S = 3 mm, T = 600 K)

Flame spread rate V_f, which is calculated from the experimental results, is shown in **Fig.9** as a function of t_w. V_f basically increases with increase of t_w, except the case for S = 12 mm. This would be due to development of flammable gas layer around the droplet array by progress of pre-evaporation. For S = 12 mm, flammable gas layer formed around each droplet would exist independently within the range of t_w studied here. In this case, time necessary for heat transfer from burning droplet to unburned droplet would be dominant factor of V_f. Therefore, V_f would not be much affected by t_w.

Also, V_f appears to approach some value with increase in t_w for d_0 =0.5 mm and S = 3 mm. In this case, pre-evaporation of the array would be most promoted in this study, since both heat capacity of each droplet and droplet interval S is the smallest in experimental conditions studied here. Considering clear blue flame at spreading flame front and large value of V_f, it is reasonable to assume propagation of premixed flame through the flammable gas layer occurrs in these cases.

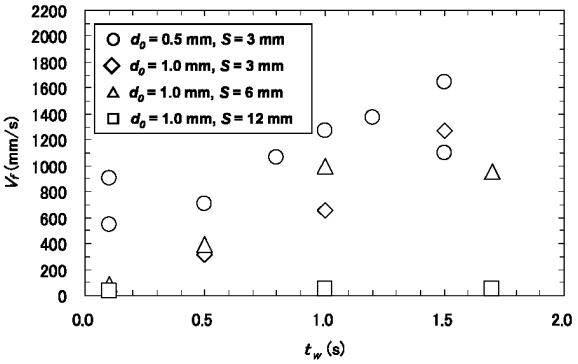

Fig.9 Flamespreadrate V_f in microgravity experiments as a function of t_w. (T = 600 K)

4. Comparison with numerical results

In this study, numerical simulation was conducted for comparison with experimental results and detail examination of flame spread mechanism. Detail numerical method is not described here, since similar method is employed in this study as our past research [7].

Numerical results are shown in **Fig.10 (a)** and **(b)** for t_w = 0 s and 1.7 s, respectively, with d_0 = 1.0 mm, S = 6 mm and T = 600 K. Temperature distribution, contours of equivalence ratio and reaction rate are indicated by gray scale, white lines and black lines, respectively. Also, t indicates the time since flame front has passed the center of the edge droplet. The flame shape in Fig.10 (a), roughly corresponds to reaction rate contours, has a qualitative agreement with the experimental results shown in Fig. 3. Also, **Fig.10 (b)** shows characteristic bow-shaped reaction region at flame front, followed by diffusion flame surrounding multiple droplets, similar as OH radical emission in Fig.7 (b).

Considering flame structure of Fig.10 (b), bow-shaped reaction region at flame front consists of lean and rich premixed flame. As a result, the flame front has a structure like a triple flame in conjunction with a diffusion flame, surrounding multiple droplets behind the bow-shaped premixed flame.

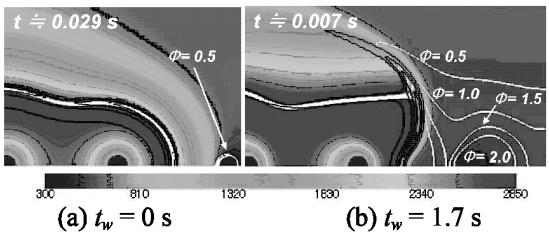

Fig.10 Contours of temperature,reaction rate,and equivalence ratio around spreading flame front. (d_0 = 1 mm, S = 6 mm, T = 600 K)

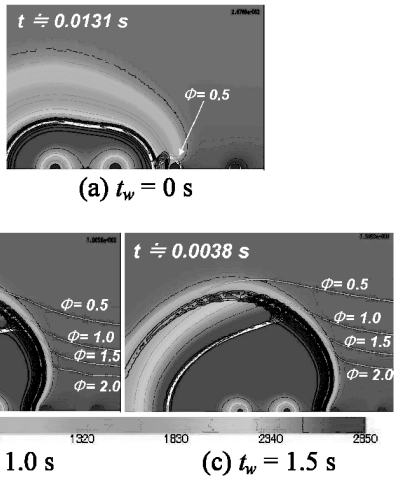

Fig.11 Contours of temperature, reaction rate, and equivalence ratio around spreading flame front. (d_0 = 0.5 mm, S = 3 mm, T = 600 K)

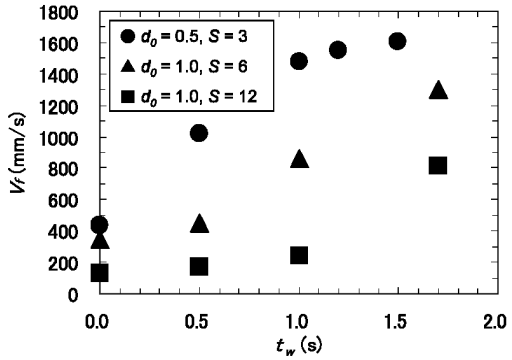

Fig.12 Flame spread rate V_f in numerical calculations as a function of t_w. (T = 600 K)

Numerical results are shown in **Fig.11 (a) ~ (c)** for t_w = 0 s, 1.0 s and 1.5 s, respectively, with d_0 = 0.5 mm, S = 3 mm and T = 600 K. Characteristic flame structure can be seen in Fig.11 (b) and (c).

These results have qualitative agreement with experimental results shown in Fig. 8.

Also, Flame spread rate V_f, which is calculated from the numerical results, is shown in **Fig.12** as a function of t_w. Basically, numerical results on V_f have good agreements with the experimental results shown in Fig. 9, not only from qualitative but also from quantitative viewpoints. However, it is obvious that the numerically calculated V_f has different trend on t_w for S = 12 mm, compared with the experimental results. For S = 12 mm, numerically calculated V_f clearly increases with inrease in t_w, although V_f in experimental results had little increase. The difference may be attributed to reaction parameters employed in numerical analysis, although further consideration is necessary.

5. Conclusions

In this study, the effects of pre-evaporation of fuel droplet array on flame spread are investigated by microgravity experiments as well as numerical simulation.

The results showed occurrence of characteristic flame structure like a triple flame with development of flammable gas layer by pre-evaporation. Also, flame spread rate V_f was significantly affected by the pre-evaporation of fuel droplet array.

In addition, numerical results basically showed good agreement with the experimental results on flame structure and V_f.

References

1) T. A. Brzustowski, A. Sobiesiak and S. Wojcicki, *Proc. Combust. Inst.* **18**, 265-273,1981.
2) S. Okajima, T. Kimoto, K. Abe and S. Yamaguchi, *Trans. Jpn. Soc. Mech. Eng.* (in Japanese), **B47** (422), 2058-2065,1981.
3) H. Kobayashi, J. Park, T. Iwahashi and T. Niioka, *Proc. Combust. Inst.* **29**, 2603-2610, 2002.
4) M. Mikami, H. Oyagi, N. Kojima, M. Kikuchi, Y. Wakashima and S. Yoda, *Combust. Flame*,**141**, 241-252, 2005.
5) M. Mikami, H. Oyagi, N. Kojima, Y. Wakashima, M. Kikuchi and S. Yoda, *Combust. Flame*, **146**, 391-406, 2006.
6) M. Kikuchi, T. Arai, S. Yoda, T. Tsukamoto, A. Umemura, M. Uchida, M. Kakei and T. Niioka, *Proc. Combust. Inst.* **29**, 2611-2619, 2002.
7) M. Kikuchi, Y. Wakashima, S. Yoda and M. Mikami, *Proc. Combust. Inst.* **30**, 2001-2009, 2005.
8) A.Umemura, *Trans. Jpn. Soc. Mech. Eng.* (in Japanese), **68**, No.672, B:2423-2428, 2002.

Received November 14, 2006
Accepted for publication, July 5, 2007